Benzodicarbomethoxy Tetrathiafulvalene Derivatives as Soluble Organic Semiconductors

Francisco Otón,[a] Raphael Pfattner,[a] Neil S. Oxtoby,[a] Marta Mas-Torrent,[a] Klaus Wurst,[b] Xavier Fontrodona,[c] Yoann Olivier,[d] Jérôme Cornil,[d] Jaume Veciana[a] and Concepció Rovira*[a]*

[a] Institut de Ciència de Materials de Barcelona (ICMAB-CSIC) and Networking Research Center on Bioengineering, Biomaterials and Nanomedicine (CIBER-BBN).Campus de la Universitat Autònoma de Barcelona, Bellaterra E-08193 (Barcelona) Spain. Fax: (+34) 935805729. E-mail: cun@icmab.es, mmas@icmab.es.

[b]Institut für Allgemeine Anorganische und Teoretische Chemie. Universität Innsbrück, A-6020, Innrain 52a, Innsbruck, Austria.

[c] Serveis Tecnics de Recerca. Universitat de Girona. Edifici Jaume Casademont (porta E), Pic de Peguera, 15.(La Creueta). E- 17003 Girona (Spain).

[d] Laboratory for Chemistry of Novel Materials. University of Mons, Place du Parc 20, B-7000 Mons.

RECEIVED DATE (to be automatically inserted after your manuscript is accepted if required according to the journal that you are submitting your paper to)

A series of new tetrathiafulvalene (TTF) derivatives bearing dimethoxycarbonyl and phenyl or phthalimidyl groups fused to the TTF core (**6** and **15-18**) has been synthesized as potential soluble semiconductor materials for organic field-effect transistors (OFETs). The electron-withdrawing substituents lower the energy of the HOMO and LUMO levels and increase the solubility and stability

of the semiconducting material. Crystal structures of all new TTF derivatives are also described and theoretical DFT calculations were carried out to study the potential of the crystals to be used in OFET. In the experimental study the best performing device exhibited a hole mobility up to 7.5 x 10^{-3} cm^2/V^1s^1.

Introduction

One of the most celebrated organic molecules for electronics, tetrathiafulvalene (TTF), was indepently reported by Wudl in 1970 and by, Coffen and Hunnig in 1971.[1] TTF and its derivatives have been thoroughly used as components of organic conductors,[2] but only recently, it has been shown that TTF derivatives are very promising materials for the preparation of OFETs owing to their processability and high device performance.[3-9] OFETs using TTFs as semiconductors have been prepared either from vacuum deposition or from solution. Soluble semiconductors are highly desired since they are compatible with low-cost deposition techniques (i.e. spin coating, ink-jet printing, etc.) and they allow for the synthesis of tailored materials. Although not suitable for practical applications, single crystals represent the ideal class of material in order to study the fundamental characteristics of organic semiconductors such as charge carrier mobility. The largest mobility in TTF OFETs have been found for single crystals prepared from solution of dithiophene-tetrathiafulvalene (DT-TTF, μ_{max} = 3.6 $cm^2V^{-1}s^{-1}$),[4] hexamethylene tetrathiafulvalene (HM-TTF, μ_{max} = 10 $cm^2V^{-1}s^{-1}$)[5] and dibenzo-tetrathiafulvalene (DB-TTF, μ_{max} = 1 $cm^2V^{-1}s^{-1}$),[6] which are among the largest reported for OFETs.

An important problem inherent to the TTF and other semiconducting materials is the degradation during operation caused by moisture and oxygen.[10] The high energy of the orbitals implicated in the transport process is the cause of the degradation, making the material more sensitive to air and humidity. A possibility to avoid this problem in a hole conducting material is to decrease the energy of the HOMO orbitals. Therefore, the inclusion of electron-withdrawing groups connected to the TTF core is a suitable approach to decrease the HOMO energy and increase the stability of the corresponding devices. [7]

Previous work[9] demonstrated that attachment of phtalimide groups to tetrathiafulvalene resulted in higher HOMO orbitals than dibenzo-tetrathiafulvalene (DB-TTF) and stable devices. Nevertheless, the solubility of the compounds was drastically reduced with respect to DB-TTF.

Herein, we report the synthesis and crystal structure of a new family of TTF derivatives containing methylester and phthalimide groups. These molecules not only bear electron-withdrawing groups fused to the TTF core to increase their electron affinity,[11] but also incorporate carbomethoxy groups that confer higher solubility in a larger range of solvents, which is important for the fabrication of solution-processed devices. The solid-state structures of all newly synthesised TTFs have also been studied by single crystal X-ray diffraction in order to assess the preferential directions for charge transport with quantum-chemical calculations.

Results and Discussion

Synthesis. The synthesis of **6** was carried out following Scheme 1. The phosponium salt **4** was synthesised by methods adapted from the literature.[12] Addition of triethylamine to an equimolar solution of compound **4** and 1,3-benzodithiolylium tetrafluoroborate (**5**) in acetonitrile resulted in the formation of the TTF **6**. The synthesis of the TTFs bearing phthalimide groups was achieved employing a different strategy. Initially, reaction of the maleimides **7-10**, prepared according to the methodology described in literature,[13] with 3,4-*bis*(bromomethyl)dithiolthione[14] resulted in the formation of the phthalimide-fused precursors **11-14**. Further reaction with 3,4-methoxycarbonyldithioltione, in a reflux of freshly distilled trimethylphosphite, led to the TTF derivatives **15-18** in a moderate yield due to the formation of homocoupling byproducts. The nature and purity of these compounds were studied by the common spectroscopic techniques (^{1}H and ^{13}C NMR, FTIR, MS and elemental analysis). Due to the low solubility of compound **18** in all tested solvents, the ^{13}C NMR spectrum could not be registered.

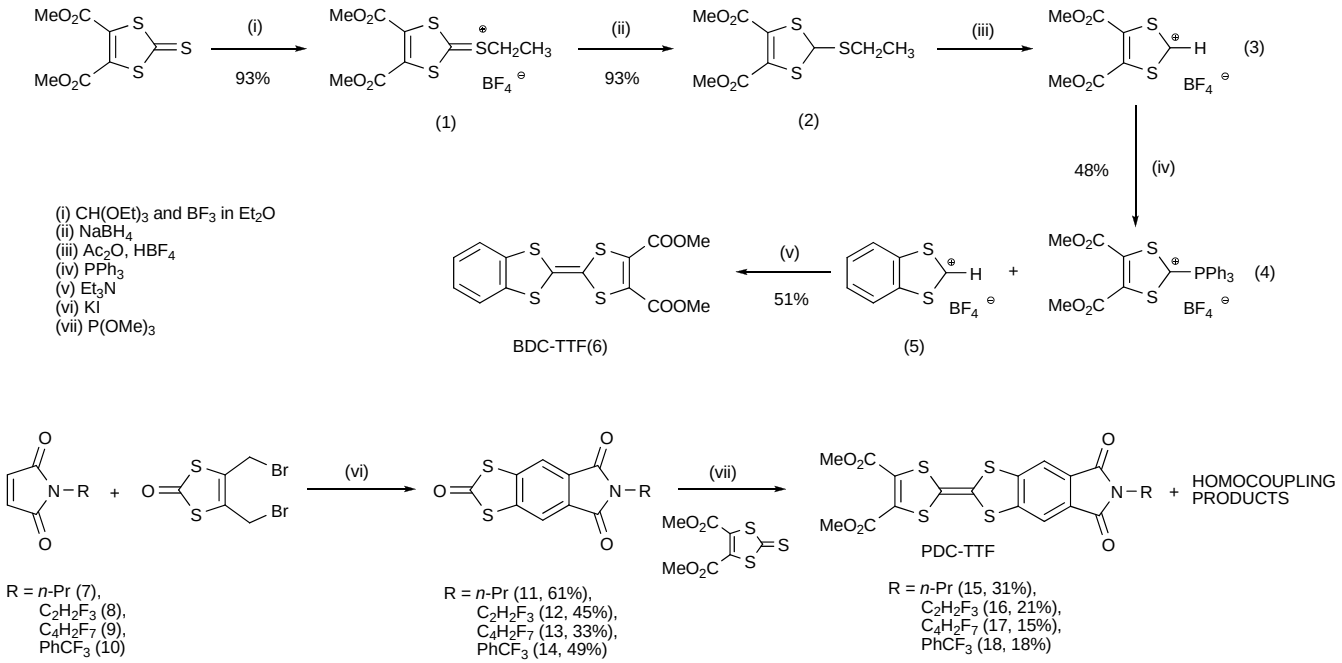

UV-Vis spectroscopy. The UV-Vis spectra of the TTF diesters **6**,**15-18** was registered in CH_2Cl_2 (c = 1x10^{-4} M). In all cases, two or three intense bands are observed in the UV region (see Table S1, Supporting Information and Figures S10 and S11). In the case of **6** only one band is observed in the visible region, which appears at λ = 441 nm. Compounds **15-18** show a band around λ = 385 nm and a broad shoulder centered in the range of λ = 460-480 nm. This band is more red shifted in the fluorine substituted molecules **16-18** due to the more electro-withdrawing character of the substituents.

The bands at lower energies are assigned to the HOMO-LUMO transition and, thus, the onset of these bands allows us to estimate the HOMO-LUMO gap[15] that, in all cases, is around 2.0 eV (see Table 1).

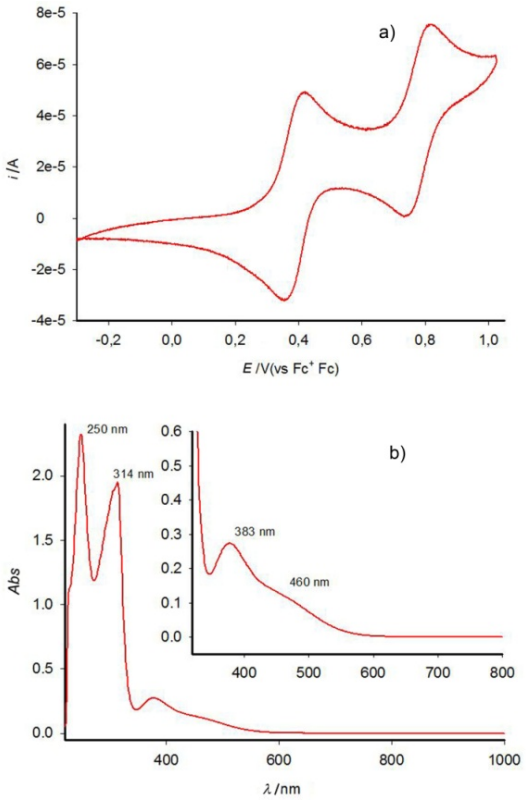

Figure 1. a) Cyclic voltammogram (CH_2Cl_2, $c = 10^{-3}$ M, TBAHP) and b) UV-Vis spectrum (CH_2Cl_2, $c = 10^{-4}$ M) of **15**.

Electrochemical properties. The redox behaviour of all synthesized compounds was studied by cyclic voltammetry (CV). Cyclic voltammograms of compounds **6** and **15-18** showed two separate reversible one-electron oxidation waves with half-wave potentials in the range $E_{1/2}^{1}$ = 0.31-0.47 V and $E_{1/2}^{2}$ = 0.76-0.81 V *vs* Fc^+/Fc (CH_2Cl_2 / 0.1 M TBAHP) (Table 1, Figure 1). The redox processes expected from the reduction of the phthalimide groups in compounds **15-18** could not be clearly observed.

As expected, the most cathodic potentials correspond to the fluorine substituted TTFs **16-18**, where the oxidation peaks appear at potentials approximately 0.15 V higher than the potentials found for **6** (Table 1). In any case, the values of the first oxidation potentials of all these compounds are considerably higher than the first oxidation potential found for the symmetric compound DB-TTF ($E_{1/2}^{1}$ = 0.17 V *vs* Fc^+/Fc),[6] which can be explained by the fact that they incorporate electron-withdrawing groups. As a consequence, these systems are expected to be more stable to oxygen exposure.

The CV experiments can be used as an experimental tool to estimate the energy of the frontier orbitals of the molecules. Therefore, from the onset of the first oxidation redox process it is possible to calculate the value of the HOMO. The value of the HOMO energy is found to be lower in the case of the phthalimide-containing compounds. Since no reduction processes were seen in the CV experiments, the estimation of the LUMO was carried out by using the HOMO-LUMO gap (*Eg*) obtained by UV-Vis spectroscopy.[15] These orbital energy levels are listed in Table 1.

The energies of the HOMO levels are in the range of -5.11 to -5.27 eV, and the energies of the LUMOs vary from -2.97 to -3.17 eV. From these values, it should be noticed that the imide moiety decreases the energy value of both HOMO and LUMO. Further incorporation of fluorinated groups also produces a small reduction of the energy of the frontier orbitals, being lower than the ones of symmetric non fluorinated dibenzotetrathiafulvalene bisimides.[9] The stabilization of HOMO is evident when compared to the one of DB-TTF, which was experimentally estimated to be around -4.97 eV.

In complement to these measurements, DFT calculations were performed with the B3LYP functional and the 6-31G* basis set in vacuum. The geometries found for the TTFs are the typical boat conformation which is usually reported in gas phase electron diffraction and theoretical calculations performed for TTF and its derivatives.[16] The HOMO of these compounds is mainly located on the TTF core and the LUMO on the electron-withdrawing groups, namely, the COOMe and the phthalimide groups (see Figures S14-S18 in Supporting Information). This displacement in the position of the LUMO clearly indicates the higher electron affinity of the imide groups substituted with fluorinated chains. The calculated energies found for the frontier orbitals of the TTF derivatives are summarized in Table 1. If no direct comparison between CV measurements and theoretical estimations of the frontier orbitals energies can be made, the trends concerning the evolution of their values are well correlated.

UV-Vis /Electrochem. DFT B3LYP/6-31G*

Table 1.

Comp	$E_{1/2\ Ox1}$[a] (V)	$E_{1/2\ Ox2}$[a] (V)	E_{HOMO} (eV)	E_{LUMO}[b] (eV)	Eg (eV)	E_{HOMO} (eV)	E_{LUMO} (eV)
6	0.31	0.78	-5.11	-2.97	2.14	-4.98	-2.01
15	0.39	0.78	-5.19	-3.02	2.17	-5.30	-2.43
16	0.46	0.76	-5.26	-3.11	2.15	-5.41	-2.59
17	0.47	0.80	-5.27	-3.17	2.10	-5.41	-2.58
18	0.46	0.81	-5.26	-3.09	2.17	-5.44	-2.64
DB-TTF	0.17	0.59	-4.97	-2.61	2.36	-4.70	-1.1210

Electrochemical and HOMO-LUMO energies of compounds **6** and **15-18**.

[a] *vs* Fc^+/Fc, in CH_2Cl_2, tetrabutylammonium hexafluorophosphate as supporting electrolyte. [b] $E_{LUMO} = E_{HOMO} + E_g$ (fom UV-Vis).

Molecular and crystal structures. Dark red single crystals of **6** with plate-like rectangular shape were grown via slow evaporation of a chlorobenzene solution. Tetrathiafulvalene **6** crystallizes in the monoclinic system, space group P2(1)/n and its structure consists of two crystallographically distinct molecules. The two molecules that compose the asymmetric unit cell are shown in Figure 2a. In both of them the benzo moiety and one methyl ester group are essentially coplanar with the TTF core and the other methyl ester group is twisted to be nearly perpendicular (73.57 and 77.70º) with respect to the TTF

core. However, though one of these molecules is fundamentally planar, the other presents a significative bending of the TTF core in the side of the ester groups (22.73º). This molecules form dimers in which the two TTF cores are nearly parallel (the angle between the planes is 2.73º) and interact via π–π and S···S interactions, with the closest S···S distance of 3.773 Å. These dimers form stacks along the *a** axis of the cell (Figure 2b). Taking the four TTF sulfur atoms as a plane for each molecule, the intra-dimer and the inter-dimer distances are 3.492 Å and 3.593 Å, respectively. The stacks further interact forming a herringbone pattern in the *a*-*b* plane (Figure 2b), in which several lateral S···S interactions occur between the stacks with distances that range from 3.596 to 3.985 Å. Simultaneously, the herringbone sheets interact through weak hydrogen bonding interactions in the *a*-*c* plane. Although esters are generally considered as hydrogen-bond acceptors, the methyl protons of the carbomethoxy groups can also act as hydrogen-bond donors.[17,18] Thus, it is interesting to note that molecules of **6** exhibit weak C-H···O hydrogen bonds between the ester moieties in the herringbone sheets [d(H(CH_3)···O(C=O) = 2.654-2.636 Å; α(C-H···O) = 170.28-109.12º; α(C=O···H) = 175.44-148.70º].

The long axis of the rectangular crystal is parallel to the *b*-crystallographic axis that exhibits numerous short intermolecular interactions, with S···S distances down to 3.606 Å to create an infinite 1D channel (Figure 2b). This can favour the charge transfer along this axis which is probed in the OFET measurements (see below).

Single crystals of the TTF-phthalimides **15-18** were also obtained by slow evaporation of chlorobenzene solutions ($CHCl_3$ in case of **17**). All these compounds crystallize in the triclinic system, in the P-1 space group. However, whereas the structures of **15, 16** and **18** are very similar and are

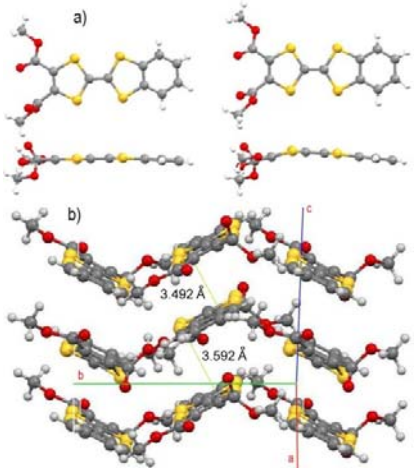

formed by one crystallographically distinct molecule, the crystal structure of **17** is completely different with a unit cell composed of two crystallographically different molecules. The formation of these two types of crystal structures can be in part due to the different nature of the solvent employed for their crystallisation.

Figure 2. a) Molecular structure of the two distinct molecules of **6**, along with the side views of them. b) Packing structure of **6** along *b*.

Compounds **15**, **16** and **18** exhibit conformations of the conjugated system where all rings in the imide side of the molecule are coplanar with the contiguous dithiol ring and present a small angle between these planes and the ones that contain the two other sulphur atoms and the carbon-carbon double bond bearing the COOMe substituents. This bending is more pronounced in **16** (11.63º). The ester groups are twisted in all cases with angles that range from 7.50 to 56.61º. As in the case of compound **6**, phthalimide-substituted TTFs **15, 16** and **18** form head-to-tail dimers that stack into columns. In all cases there are similar intra-dimer and inter-dimer distances (plane-to-plane distances between 3.50 and 3.69 Å for all of them). Nevertheless, they differ in the longitudinal shifting of the molecules in the intra- and inter-dimers (see Figure 3) and as a consequence, there are large differences in the sulphur-sulphur distances, which are for the intra-dimer pairs 3.960, 3.714 and 3.807 Å for **15**, **16** and **18**, respectively. However, there are no short S···S distances in the inter-dimer structures, and neither between different columns. Probably the most significant difference in the crystals is the lateral packing of the columns. Compound **15** exhibits an almost planar head-to-tail packing with the nearest neighbour molecules in the adjacent stacks, whereas in compounds **16** and **18** the packing is head-to-head (Figures S19-S22 in Supporting Information).

As found for **6**, several weak hydrogen bonds are observed in these crystals, especially between the imide CO groups and the aromatic protons and the ester CO groups and the terminal CH_3 groups (choosing **15** as an example, this compound exhibits weak C-H···O hydrogen bonds between imides and the phenyl rings [d(Ph-H···O=C-N) = 2.409 Å; α(C-H···O) = 125.25º], between the esters and phenyl

rings [d(Ph-H···O=C-O) = 2.288 Å; α(C-H···O) = 152.55º], and between ester groups and the alkyl chain [d(CH-H···O) = 2.596-2.627 Å; α(C-H···O) = 150.65º-167.05º]). In compounds **16** and **18** short F···H interactions have been also found.

Indexing measurements of crystals of **15**, **16** and **18** show that the longest axis of the crystal coincides with the growing direction of the columns, whose relation with the crystallographic axis is different in all cases.

Compound **17** has two crystallographically distinct molecules that are fundamentally planar and form an angle of 71.7º between them. The packing of one of these molecules is similar to the other phthalimide-TTF derivatives exhibiting a columnar structure of dimers (Figure 5a), but the other molecules form a layer of dimers with their face almost perpendicular to the adjacent units of the columns (see Figure S21, Supporting Information). Inside the columns, the intra-dimer and inter-dimer S···S distances are 3.998 and 4.541 Å and the plane-to-plane distances are 3.529 and 3.599 Å, respectively. These distances are slightly longer than in the other phthalimide substituted TTFs studied here. Despite the fact that the packing of **17** is considerably more complex, the nature of the hydrogen bonds is similar.

Indexation measurements of crystals of **17** show that the longer axis of the crystal coincides with the crystallographic *a* axis, that is the stacking direction of the columns.

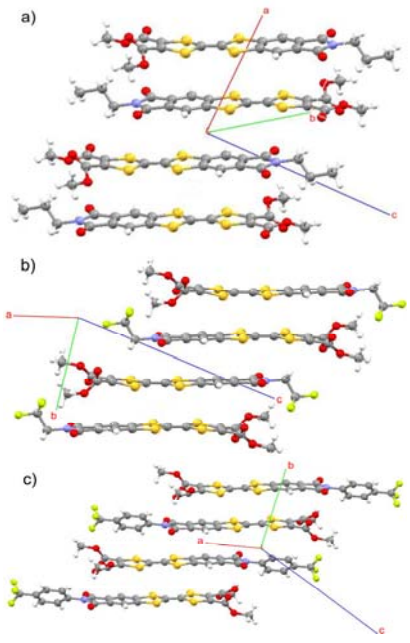

Figure 3. Views of the crystal structure of compounds a) **15,** b) **16** and c) **18** showing the formation of columns of head to tail dimers.

Theoretical characterisation of charge transport properties. At a microscopic level, a hopping mechanism is often a good starting point to describe theoretically charge transport of organic semiconductors in operating devices.[19] The charge transfer rate k_{hop} between two interacting molecules can be evaluated with the help of Marcus-Levich-Jortner (M-L-J) theory as:[20]

$$k_{hop} = \frac{2\pi}{\hbar} t^2 \sqrt{\frac{1}{4\pi\lambda_S k_B T}} \sum_{n=0}^{\infty} \exp(-S) \frac{S^n}{n!} \exp\left[-\frac{(\Delta G^0 + \lambda_S + n\hbar\omega_i)^2}{4\lambda_S k_B T} \right]$$

The rate constant depends on several parameters accessible from quantum-chemical calculations:

- the transfer integral t which depicts the strength of the interactions between the electronic levels (HOMO for holes and LUMO for electrons) of the molecules involved in the charge transfer process. This parameter has been calculated at the Density Functional Theory (DFT) level with the B3LYP functional and a TZP basis set, using the fragment approach implemented in the ADF package with the methodology described in Ref 21.

- S is the Huang-Rhys factor associated to a single effective intramolecular vibrational mode (with a typical energy ħω of a stretching mode set here to 0.2 eV) that assists the charge transfer by allowing for tunneling across the energy barrier. With a single mode, S is directly related to the internal reorganization energy λ_i (= $S \cdot \hbar\omega$) that reflects the degree of geometric changes in the molecules upon addition of a charge;[22] λ_i is often computed at the DFT level with the B3LYP functional and a 6-31G(d,p) basis set due to the good agreement observed with values extracted from Ultraviolet Photoemission Spectroscopy spectra.[23]

- λ_s is the external reorganization energy that accounts for the nuclear displacements in the surrounding medium and the resulting electronic effects.[24] This parameter cannot be easily accessed

from quantum-chemical calculations though values in the range between 0.2 and 0.3 eV are obtained from simple models based on a dielectric continuum.[25] We will set here λ_s equal to a value 0.2 eV in all crystals; we stress that the main conclusions of this work remain valid for other values of λ_s.

- when neglecting entropic contributions, the Gibbs energy ΔG^0 accounts for the difference in energy between the initial and final states involved in the charge transfer process. Since a weak energetic disorder is expected in single crystals, we have considered only the impact of the external electric field. In this case, ΔG^0 is expressed as $\Delta G^o = e \cdot \vec{F} \cdot \vec{d}$, with $\vec{F}$ and $\vec{d}$ the electric field and separation vectors between mass centers, respectively.

The Marcus expression shows that high transfer rates require large transfer integrals and small reorganisation energies. Interestingly, the internal reorganisation energy for positive polaron is found to be around 350 meV for each compound. The addition of imide group or different side chains has thus no significant impact on this parameter. A deeper analysis of the bond-length modification upon oxidation shows that the main changes are systematically located over the TTF core leading to the appearance of a quinoid structure. Note that such λ_i values are significantly larger than that calculated at the same level of theory for pentacene (~ 100 meV)[23] and DB-TTF (250 meV), a symmetric compound of the family. However, a theoretical study on DT-TTF showed that when the local molecular environment is taken into account in DT-TTF (i.e. including in the calculation a cluster of molecules instead of a single one) and the charge can be partially delocalised over several molecules, the value of the reorganisation energy is significantly reduced. This behaviour can also be expected to take place in other TTF derivatives.[2d,26]

Previous theoretical works[25,27] have shown that the magnitude of the transfer integral is driven by the shape of the molecular orbitals as well as by the relative position of the molecules involved in the charge transfer. We have thus calculated the transfer integrals for all possible directions in the crystalline structures and have reported hereafter only the non-negligible contributions (larger than 1 meV).

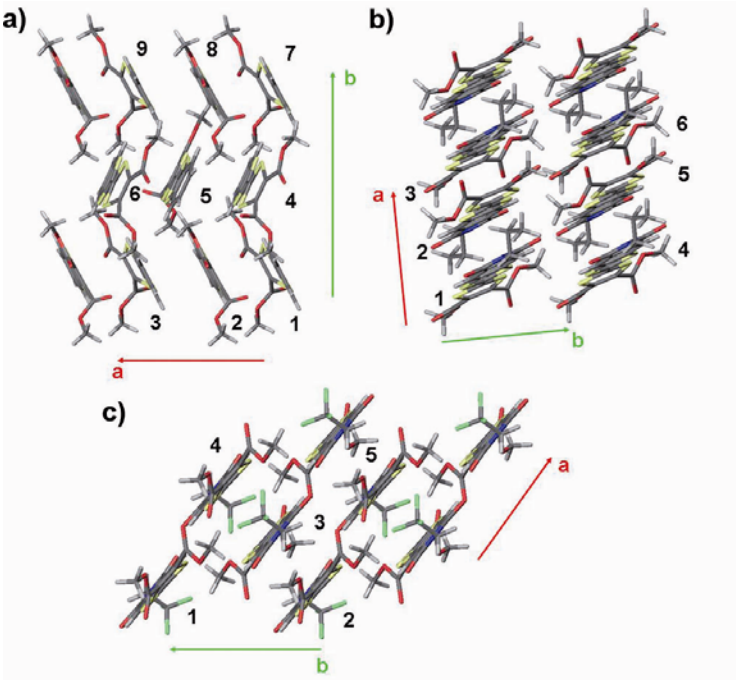

Figure 4. *a*-*b* plane structures of compounds **6** (a), **15** (b) and **16** (c) extracted from the X-ray spectra to calculate the transfer integrals and charge carrier mobility values.

Compound **6** exhibits its largest transfer integrals (on the order of 20 meV) along the *a* and diagonal axes within the *a*-*b* plane (Figure 4a). A slight difference is calculated along the *a* axis between adjacent molecules due to the head-to-tail configuration; this promotes transfer integrals of 18 meV *versus* 23.5 meV for the intra- and inter-dimer jumps, respectively. Although molecules **15**, **16**, and **18** display similar crystalline structures (Figures 4b, 4c, and 5b), the calculated transfer integrals are sensibly different in magnitude and have systematically their most important contributions along the intra-columnar direction, with the larger value obtained for the intra-dimer jump (24, 58, and 103 meV for **15**, **16** and **18**, respectively). The inter-dimer transfer is also characterised by non-negligible transfer integral values (12, 33, and 34 meV for **15**, **16** and **18**, respectively), thus ensuring that the intra-columnar direction is a favourable direction for charge transport. Smaller but non-negligible transfer integrals are also calculated along the inter-columnar direction (*b* and diagonal axes of the *a*-*b* plane for compound **15** and directions *d*(1,3) and *d*(3,5) for compounds **16** and **18**, see Figures 4a, 4b and 5b).

As mentioned before, compound **17** exhibits a quite different packing compared to the other molecules (Figure 5a). The *a*-*b* plane is made of a juxtaposition of columns of different types promoting face-to-face or side-to-side configurations. The transfer integrals in face-to-face configurations are different for the intra-dimer (13 meV, dimer 1-2) *versus* inter-dimer (67 meV, dimer 2-3) jump, as expected from the head-to-tail geometry. Very small contributions are found along the side-to-side direction (6 meV, dimer 6-7) whereas significant values are calculated for the dimers 7-8 and 7-9. Moreover, inter-columnar charge transfer is expected to occur in view of the significant transfer integrals calculated in dimers 3-7, 4-7, and 5-7 (67, 30, and 13 meV, respectively). Note that the pathways are equivalent in dimers 8-10, 8-11, 8-12 due to the symmetry of the crystal. For all derivatives under study, it turns out that transfer integrals between molecules located in different layers are very small so that charge transport has a two-dimensional character.

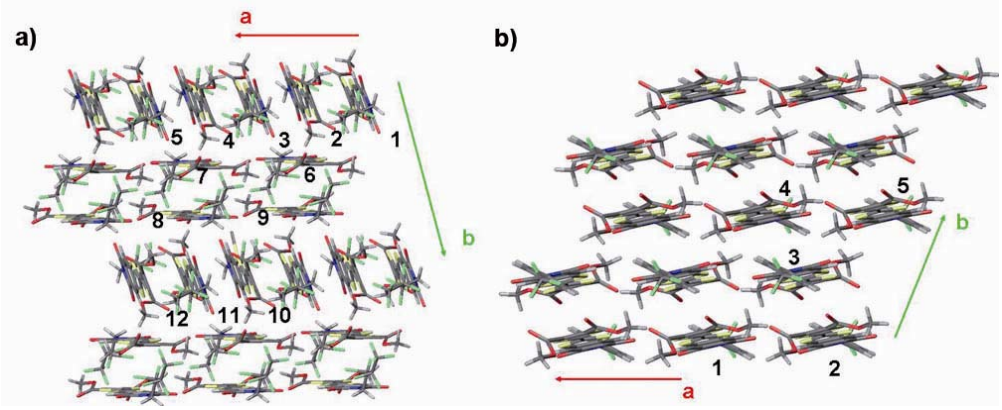

Figure 5. *a*-*b* plane structures of compounds **17** (a) and **18** (b) extracted from X-ray diffraction spectra to calculate transfer integrals and charge carrier mobility values.

Several experimental studies[28] have nicely shown that the charge carrier mobility in single crystals is generally not isotropic due to the high sensitivity of electronic couplings to molecular packing. Monte-Carlo simulations have thus been performed in order to characterise the anisotropy of the hole mobility

for the different TTF derivatives. These simulations propagate a single charge carrier in the crystals along directions chosen according to the transfer probability p_{ij}:[29]

$$p_{ij} = \frac{k_{ij}}{\sum_{l} k_{il}}$$

where k_{ij} is the transfer rate between molecules *i* and *j* and the sum runs over all neighbours of the molecule supporting the charge. The charge carrier mobility is ultimately evaluated from the total distance d_{tot} travelled by the charge during the simulation, the total time t_{tot} of the simulation (linked to the individual hopping times and hence inverse of the individual transfer rates) and electric field norm:

$$\mu = \frac{d_{tot}}{t_{tot} \cdot F}$$

The mobility anisotropy curve is then generated by repeating this scheme for different orientations of the electric field. An electric field of 1000 V/cm similar in magnitude to that typically applied in field-effect transistors is considered here.

As expected, compounds **15**, **16,** and **18** have their maximum hole mobility value (Figure S27, Figure S28 and Figure S29) along the intra-columnar direction. This is driven by the large difference between the transfer integrals along the intra- and inter-columnar directions, leading to a ratio of the mobility around 4.5, 2, and 8, respectively. In spite of the small transfer integral values along the inter-columnar direction (*b*-axis) in **6**, the mobility value is maximized along this axis (Figure 6a). The simulations indicate that the holes migrate with a zig-zag motion along the diagonal axes to yield the largest mobility component along the *b* axis. The anisotropy is weak for this compound since the transfer integrals have the same order of magnitude along the *a* and diagonal directions. In spite of the tight packing of molecule **17** within the columns along the *a* axis, the simulations reveal a mobility maximum along the inter-columnar direction (deviation of 70 degrees compared to the measurement direction, see Figure 6b). This is rationalized by the presence of efficient inter-columnar pathways, as discussed previously.

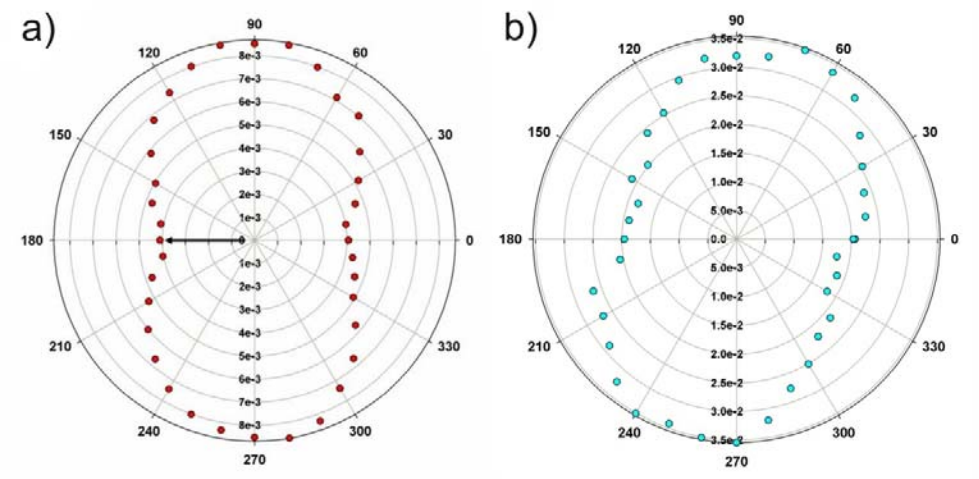

Figure 6. Anisotropy mobility curves in the *a*-*b* plane of the crystalline structure of **6** (a) and **17** (b). The 0 degree orientation corresponds to the *a* axis. The black arrows depict the intra-columnar direction. The mobility values are expressed in $cm^2V^{-1}s^{-1}$.

Single-crystal field-effect transistor devices. OFETs were fabricated on thermally oxidized silicon substrates. Crystals were formed on the substrate by drop casting a solution of 0.5- 1.0 mg of the compounds in 1 ml of toluene or chlorobenzene and allowing the solvent to evaporate slowly under darkness and reduced ambient humidity. Only **6** gave crystals good enough to give reliable measurements. Some of the long plate-like crystals formed were connected with graphite paste (Figure 7).

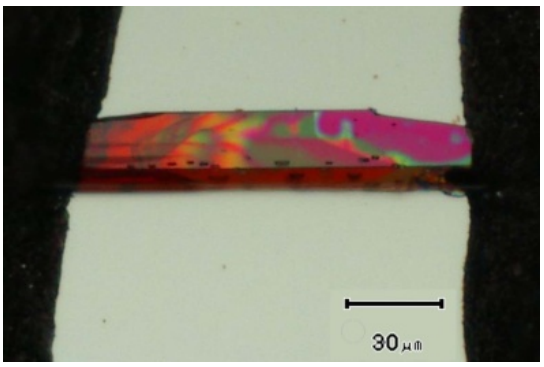

Figure 7. Optical microscopy photograph of the BDC-TTF **6** top-contact OFET with graphite source and drain electrodes. The channel length and width are 122 and 20 μm, respectively.

Figure 8 shows the source-drain current I_{SD} of **6** versus the applied source-drain voltage V_{SD} across the two graphite electrodes for different gate voltages V_G applied to the silicon substrate, which acts as a bottom gate. The resulting graphs are typical of a p-type semiconductor since as a more negative V_G is applied, more holes are induced in the semiconductor and the conductivity increases. When a -60 V gate voltage is applied a clear saturation behaviour at V_{SD} = -20 V is observed. The hole field-effect mobility was calculated according to the formula described in the experimental section and the mobility found in the saturation regime at V_{SD} = -40 V was of 7.5 x 10^{-3} $cm^2V^{-1}s^{-1}$ (V_{TH} = -27.6 V; on/off = 80) which is in the order of the one predicted theoretically (Figure 6 i). The stability of these devices was tested measuring the electrical properties every week along a month in which the devices were stored in room conditions. In this period, no degradation of the mobility was observed, and only a small doping effect caused the shifting of threshold voltage from -27.6 V to 28 V.

Interestingly, we should notice that the OFET measurements were carried out along the longest crystal axis (parallel to *b*) where the calculations predict the best transport pathways. This direction does not correspond to the face-to-face packing of the molecules like in the high mobility semiconductors DB-TTF and DT-TTF, but is promoted through a diagonal zig-zag pathway where one of the most prominent features is the presence of short S···S contacts. This result is in agreement with the fact that π-stacking is not the only assembly that can result in effective orbital overlap, as it has been discussed by Brédas and col.[30] Indeed, in other TTF derivatives lateral S···S have also been found to give rise to high charge carrier mobilities.[3b, 5, 31]

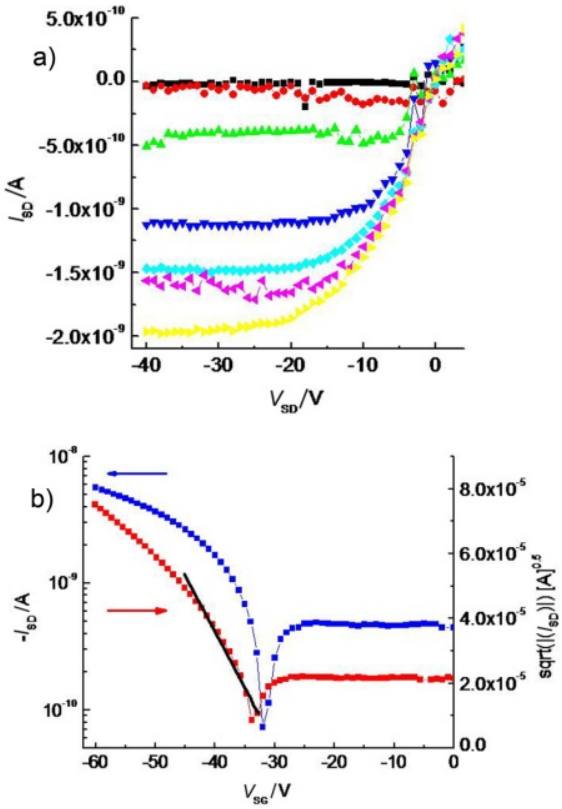

Figure 8: a) I_{SD} *versus* V_{SD} at V_G (from top to bottom) 0, -10, -20, -30, -40, -50, -60 V for a single crystal OFET based on **6**. b) Transfer characteristics at V_{SD}= -40V for this device.

Conclusion

In summary, we have described the synthesis and crystal structure of a series of tetrathiafulvalene derivatives bearing electron-witdrawing groups as esters and imides. These groups contribute to reduce the energies of frontier orbitals and the HOMO-LUMO gap of these compounds when compared to other TTF derivatives used as semiconductors such as DB-TTF and DT-TTF. The incorporation of the ester groups have the additional advantage of imparting good solubility to the compounds, permitting the preparation of OFET devices with single crystals of the TTF derivatives grown from solution, and giving an improved stability to de prepared devices. In all cases, the crystal structure of the compounds shows slip-stacks of dimers in contrast with the TTF derivatives that are symmetrically substituted such as DB-TTF[32] and dibenzotetrathiafulvalene bisimides,[9] in which regular columns of molecules are formed. The DFT quantum-chemical calculations carried out point to relatively high reorganization energy in all compounds. Furthermore, the computed values of the transfer integrals show wide

variations with non negligible transfer integrals calculated along specific directions that not always correspond to the π-π stacking of the molecules. In the tested conditions, the best OFET performance with μ = 7.5 x 10^{-3} $cm^2V^{-1}s^{-1}$ have been found in devices prepared with a single crystal of **6** in a top contact configuration using graphite paste as source and drain electrodes. Undoubtedly, the search for novel soluble organic semiconductors is a crucial step in order to progress in the field.

Experimental Section

Materials and Methods. All reactions were carried out under Ar and using solvents which were dried by routine procedures. *Bis(*bromomethyl)dithiolone,[14] 3,4-methoxicarbonyldithiol-tione[29] and phosphonium salt **4**[12] were synthesized using procedures reported in the literature. Graphite paste XC-12 was purchased from Dotite and thermally grown silicon dioxide was purchased from Si-Mat.

Reagents obtained from commercial sources were used without further purification. Column chromatography was performed using silica gel (60 A C.C. 35-70 μm, sds) as the stationary phase. ^1H and ^{13}C NMR (250, 360 and 400 MHz) spectra were recorded on Bruker spectrometers. The following abbreviations for stating the multiplicity of the signals in the NMR spectra were used: s (singlet), d (doublet), t (triplet), m (multiplet), q (quaternary carbon). The MALDI-TOF MS spectra were recorded on a Bruker Ultraflex II TOF spectrometer. Infrared spectra were recorded on a Perkin-Elmer FT-IR Spectrum One spectrometer. UV-Vis spectra were performed in CH_2Cl_2 (c = 1 x 10^{-4} M) using a VARIAN CARY 5000 spectrophotometer. Elemental analyses were carried out on a Carlo Erba CE 1108 Elemental Analyser.

Cyclic Voltammograms were performed with a conventional three-electrode configuration consisting of platinum working electrode and auxiliary electrodes and Ag/AgCl reference electrode. The experiments were carried out with a 10^{-3} M solution of the corresponding TTF derivative in CH_2Cl_2 containing 0.1 M (n-$C_4H_9)_4PF_6$ (TBAHP) as supporting electrolyte. Deoxygenation of the solutions was achieved by bubbling nitrogen for at least 10 min and the working electrode was cleaned after each run. The CVs were recorded with a scan rate increasing from 0.05 to 1.00 Vs^{-1}. Ferrocene was used as an

internal reference both for potential calibration and for reversibility criteria. All of the potential values reported are relative to the Fc^+/Fc couple at room temperature. Under these conditions the ferrocene has a redox potential E^0 = 0.440 V *vs* Ag/AgCl sat. electrode and the anodic-cathodic peak separation is 67 mV. Crystallographic data of **6** were measured with a Nonius Kappa CCD diffractometer with monochromatic Mo-Kα (λ=0.71073 Å) radiation. Data were collected via ϕ and ω multiscans and reduced with the program DENZO-SMN without absorption correction. The structure was solved with direct methods SHELXS86 and refined against F^2 with SHELXL97. Crystallografic data of **15-18** were measured in a Bruker SMART Apex CCD using graphite-monocromated Mo Kα radiation (λ = 0.71073 Å) from an X-Ray Tube. The measurements were made in the range 2.44 to 28.22° for θ. Full-sphere data collection was carried out with φ and ω scans. Programs used: data collection, Smart version 5.631 (Bruker AXS 1997-02); data reduction, Saint + version 6.36A (Bruker AXS 2001); absorption correction, SADABS version 2.10 (Bruker AXS 2001). Structure solution and refinement was done by using SHELXTL Version 6.14 (Bruker AXS 2000-2003). The structure was solved by direct methods and refined by full-matrix least-squares methods on F^2. The non-hydrogen atoms were refined anisotropically. The H-atoms were placed in geometrically optimized positions and forced to ride on the atom to which they are attached.

Computational Details. Geometries were fully optimized with tight convergence criteria at the DFT level with the Gaussian 03 package (E01 release),[33] using the B3LYP[34] functional and the 6-31G(d) basis set. All energies are not corrected for the zero-point vibrational energy. The electronic structures and the reorganization energies were calculated at the same level of theory.

Synthesis of *BDC-TTF* (6). A solution of **4**[12] (3.234 g, 5.7 mmol) and 1,3-benzodithiolylium tetrafluoroborate (1.405 g, 5.8 mmol), in dry acetonitrile (45 ml) was stirred for 30 min under argon. Dry triethylamine (5 ml) was added to this solution and the resulting mixture was stirred overnight. The red solid that precipitates was filtered and recrystallised from methanol to yield a red crystalline solid (1.097 g, 3.0 mmol, 51%) that was characterized as **6**.

Yield: 51%; m.p. 177-178 ºC; δ_H(500 MHz; $CDCl_3$; Me_4Si) 7.25 (m, 2H, Ar), 7.13 (m, 2H, Ar), 3.84 (s, 6H); δ_C(160.4 MHz; $CDCl_3$) 160.1 (q, CO), 136.4 (q, Ar), 132.1 (q, Ar), 126.3 (CH, Ar), 122.1 (CH, Ar), 113.2 (q, S-C=C), 107.4 (q, S-C=C), 53.5 (CH_3); ν_{max}(KBr)/cm^{-1} 3059, 1739, 1717, 1581, 1566, 1433, 1251 , 1090, 1020, 767, 739, 676; *m/z* (MALDI) 369.9 (100, M^+). Elemental analysis calcd (%) for $C_{14}H_{10}O_4S_4$: C, 45.39; H, 2.72; S, 34.62; found C, 45.48; H, 2.99; S, 34.37.

General procedure for the synthesis of phthaloyldithiolones (11-14). A solution of the corresponding N-substituted maleimide (**7-10**, 4.10 mmol) and 3,4-*bis*(bromomethyl)dithiolone (8.20 mmol), in dry DMF (25 ml), was refluxed for 8 hours under argon. Then, the solvent was partially removed under vacuum and the residue mixed with water and extracted with *n*-hexane/diethylether (8:2). The organic solvent was removed under vacuum and the solid chromatographed on a silica gel column (CH_2Cl_2, Rf = 0.4-0.6). The resulting white solids were characterized as pure compounds **11-14**.

11. Yield: 61%; m.p. 225-226 ºC; δ_H(250 MHz; $CDCl_3$; Me_4Si) 7.97 (s, 2H), 3.67 (t, 2H, ^3J(H,H) = 7.2Hz), 1.73-1.67 (m, 2H), 0.95 (t, 3H, ^3J(H,H) = 7.2 Hz); δ_C(80.2 MHz; $CDCl_3$) 187.2 (q, S-C=O), 166.9 (q, N-C=O), 138.4 (q, Ar-S), 130.4 (q, Ar-C), 117.8 (CH, Ar), 40.0 (CH_2-N), 21.8 (CH_2), 11.3 (CH_3); ν_{max}(ATR)/cm^{-1} 3015, 2974, 1766, 1696, 1601, 1463, 1436, 1390, 1335, 1203, 1189, 1144, 1099, 1057, 973, 919, 875, 851, 765, 746; *m/z* (MALDI) 252 (100, M^+-27, +H –CO); Elemental analysis calcd (%) for $C_{12}H_9NO_3S_2$: C, 51.60; H, 3.25; N, 5.01; S, 22.96; found C, 51.48; H, 3.19; N, 4.95; S, 22.80.

12. Yield: 45%; m.p. 161-162 ºC; δ_H(250 MHz; $CDCl_3$; Me_4Si) 8.02 (s, 2H), 4.30 (q, 2H, ^3J(H,F) = 8.5Hz); δ_C(80.2 MHz; $CDCl_3$) 186.7 (q, S-C=O), 165.2 (q, N-C=O), 139.5 (q, Ar-S), 129.6 (q, Ar-C), 123.0 (q, q, ^1J(C,F) = 356.9 Hz), 118.4 (CH-Ar), 39.2 (CH_2, q, ^2J(C,F) = 46.9 Hz); δ_F(376.3 MHz; $CDCl_3$; $CFCl_3$) -70.45; ν_{max}(ATR)/cm^{-1} 3010, 2983, 1779, 1757, 1722, 1651, 1417, 1387, 1333, 1260, 1208, 1162, 1066, 905, 890, 858, 834, 746; *m/z* (MALDI) 292 (100, M-27, +H –CO); Elemental analysis calcd (%) for $C_{11}H_4F_3NO_3S_2$: C, 41.38; H, 1.26; N, 4.49; C, 20.09. found: C, 41.39, H, 1.17; N, 4.29; S, 19.99.

13. Yield: 33%; m.p. 126-127 ºC; δ_H(250 MHz; $CDCl_3$; Me_4Si) 8.06 (s, 2H), 4.38 (t, 2H, ^3J(H,F) = 15.2 Hz); δ_C(80.2 MHz; $CDCl_3$) 186.7 (q, S-C=O), 165.3 (q, N-C=O), 139.5 (q, Ar-S), 129.6 (q, Ar-C), 118.4 (CH-Ar), 37.4 (CH2, q, ^2J(C,F) = 32.3 Hz); δ_F(376.3 MHz; $CDCl_3$; $CFCl_3$) -80.50 (t, ^3J(F,F) = 10Hz), -116.86 (m), -127.51 (m); ν_{max}(ATR)/cm^{-1} 3096, 3014, 2968, 1786, 1732, 1660, 1418, 1386, 1354, 1314, 1282, 1228, 1181, 1122, 1068, 1029, 1011, 959, 928, 897, 834, 794, 750; *m/z* (MALDI) 392 (100, M-27, +H –CO); Elemental analysis calcd (%) for $C_{13}H_4F_7NO_3S_2$: C, 37.24; H, 0.96; N, 3.34; S, 15.29; found: C, 37.15; H, 0.95; N, 3.26; S, 15.16.

14. Yield: 49%; m.p. 187-188 ºC; δ_H(250 MHz; $CDCl_3$; Me_4Si) 8.09 (s, 2H), 7.77 (d, 2H, ^3J(H,H) = 8.5 Hz), 7.62 (d, 2H, ^3J(H,H) = 8.5 Hz); δ_C(80.2 MHz; $CDCl_3$) 190.5 (q, S-C=O), 176.6 (q, N-C=O), 134.5 (q, Ar-S), 130.9 (q, ^2J(C,F) = 41.7 Hz, Ar-CF_3), 126.5 (CH, Ar), 126.4 (CH, Ar), 126.3 (q, Ar), 126.1 (q, Ar), 124.1 (CH, Ar), 123.5 (q, ^1J(C,F) = 349.3 Hz, CF_3); δ_F(376.3 MHz; $CDCl_3$; $CFCl_3$) -62.85; ν_{max}(ATR)/cm^{-1} 2927, 1786, 1705, 1649, 1616, 1588, 1518, 1417, 1386, 1318, 1179, 1161, 1125, 1106, 1064, 1020, 956, 912, 882, 835, 769, 755; *m/z* (MALDI) 354 (100, M-27, +H-CO); Elemental analysis calcd (%) for $C_{16}H_6F_3NO_3S_2$: C, 50.39; H, 1.59; N, 3.67; S, 16.82; found C, 50.28; H, 1.51; N, 3.78; S, 16.89.

General procedure for the synthesis of PDC-TTF (15-18). A solution of the corresponding dithiolones **11-14** (0.58 mmol) and 3,4-methoxicarbonyldithioltione (0.87 mmol), in freshly distilled $P(OCH_3)_3$ (15 ml) was stirred for 6 hours under argon. Then, the solvent was removed under reduced pressure and the residue was purified by column chromatography on a silica gel (AcOEt : *n*-Hex 1 : 1, Rf = 0.5-0.7). The red-orange solids were recrystallized from $CHCl_3$.

15. Yield: 31%; m.p. 233-234ºC; δ_H(250 MHz; $CDCl_3$; Me_4Si) 7.65 (s, 2H), 3.86 (s, 6H), 3.62 (t, 2H, ^3J(H,H) = 7.2 Hz), 1.72-1.65 (m, 2H), 0.93 (t, 2H, ^3J(H,H) = 7.2 Hz); δ_C(80.2 MHz; $CDCl_3$) 167.1 (q, COO), 159.6 (q, N-C=O), 143.3 (q, Ar-S), 131.8 (q), 130.4 (q), 116.2 (CH, Ar), 111.2 (q, S-C=C), 109.5 (q, S-C=C), 53.5 (CH_3-O), 39.8 (CH_2-N), 21.8 (CH_2), 11.3 (CH_3); ν_{max}(ATR)/cm^{-1} 2952, 1761, 1734, 1699, 1573, 1434, 1391, 1365, 1287, 1229, 1206, 1189, 1053, 1015, 965, 907, 765, 745; *m/z* (MALDI)

480 (100, M⁻1); Elemental analysis calcd (%) for $C_{19}H_{15}NO_6S_4$: C, 47.39; H, 3.14; N, 2.91; S, 26.63; found: C, 47.23; H, 3.06; N, 2.80; S, 26.51.

16. Yield: 21%; m.p. 253-254 ºC; δ_H(250 MHz; $CDCl_3$; Me_4Si) 7.72 (s, 2H), 4.27 (q, 2H, ^3J(H,F) = 8.5 Hz), 3.87 (s, 6H); δ_C(80.2 MHz; $CDCl_3$) 165.4 (q, COO), 159.6 (q, N-C=O), 144.6 (q, Ar-S), 131.8 (q), 129.7 (q), 116.7 (CH, Ar), 112.1 (q, S-C=C), 108.8 (q, S.C=C), 53.5 (CH_3-O), 39.1 (CH_2-N, ^2J(C,F) = 46.5 Hz); δ_F(376.3 MHz; $CDCl_3$; $CFCl_3$) -70.52; ν_{max}(ATR)/cm^{-1} 2950, 1780, 1728, 1634, 1436, 1385, 1264, 1164, 1067, 874, 748; *m/z* (MALDI) 521 (100, M^+); Elemental analysis calcd (%) for $C_{18}H_{10}F_3NO_6S_4$: C, 41.45; H, 1.93; N, 2.69; S, 24.59; found C, 41.39; H, 1.81; N, 2.60; S, 24.39.

17. Yield: 15%; m.p. 247-248 ºC; δ_H(250 MHz; $CDCl_3$; Me_4Si) 7.73 (s, 2H), 4.33 (t, 2H, ^3J(H,F) = 15.2 Hz), 3.87 (s, 6H); δ_C(80.2 MHz; DMSO-d^6) 166.0 (q, COO), 159.4 (q, N-C=O), 143.7 (q, Ar-S), 131,3 (q), 129.8 (q, Ar-C), 118 (CH, Ar) 112.2 (q, S-C=C), 109.3 (q, S-C=C), 54.0 (CH_3-O); δ_F(376.3 MHz; $CDCl_3$; $CFCl_3$) -80.52(t, ^3J(F,F)=10Hz), -116.90 (t, ^3J=9.4Hz), -127.54 (m); ν_{max}(ATR)/cm^{-1} 3017, 2961, 1781, 1744, 1726, 1588, 1577, 1436, 1386, 1351, 1264, 1223, 1176, 1121, 1086, 1064, 1032, 956, 916, 886, 795, 772, 749, 734; *m/z* (MALDI) 621 (100, M^+); Elemental analysis calcd (%) for $C_{20}H_{10}F_7NO_6S_4$: C, 38.65; H, 1.62; N, 2.25; S, 20.64; found: C, 38.61; H, 1.50; N, 2.16; S, 20.50.

18. Yield: 18%; M.p. 251-252 ºC; δ_H(250 MHz; $CDCl_3$; Me_4Si) 7.78 (s, 2H), 7.76 (d, 2H, ^3J(H,H) = 8.5 Hz), 7.62 (d, 2H, ^3J(H,H) = 8.5 Hz), 3.87 (s, 6H); δ_F(376.3 MHz; $CDCl_3$; $CFCl_3$) -62.68; ν_{max}(ATR)/cm^{-1} 2957, 1773, 1738, 1716, 1615, 1579, 1436, 1361, 1320, 1288, 1265, 1171, 1115, 1068, 1037, 1020, 934, 905, 840, 769, 739; *m/z* (MALDI) 583 (100, M^+); Elemental analysis calcd (%) for $C_{23}H_{12}F_3NO_6S_4$: C, 47.33; H, 2.07; N, 2.40; S, 21.98; found: C, 47.40; H, 2.00; N, 2.30; S, 22.07.

Crystal structures. (For a more detailed description see Supporting Information). **6**. $C_{14}H_{12}O_8S_4$, *Mr* =370.46, monoclinic, P21/c, a =8.3891(4) Å, b = 10.8253(3) Å, c =34.158(1) Å, α =90º, β = 95.085 (2)º, γ= 90º, *V* = 3089.83(19) $Å^3$, Z = 8, R1 = 0.0461, wR2 = 0.0986, *T* =233(2) K. **15**. $C_{19}H_{15}NO_6S_4$, *Mr* = 481.56, Triclinic, P-1, a = 8.796(4) Å, α = 74.506(8)º, b = 9.291(4) $Å^3$, β = 89.266(8)º, c = 13.986(7) $Å^3$, γ = 69.251(8)º, *V* = 1025.8(8) $Å^3$, Z = 2, R1 = 0.0456, wR2 = 0.1272, *T* = 300(2) K. **16**.

$C_{18}H_{10}F_3NO_6S_4$, *Mr* = 521.51, Triclinic, P-1, a = 7.893(3) Å, α = 92.716(7)º, b = 8.096(3) Å, β = 100.458(6)º, c = 16.569(6) Å, γ = 107.625(6)º, *V* = 986.4(6) Å^3, Z = 2, R1 = 0.0423, wR2 = 0.0894, *T* = 300(2) K. **17**. $C_{20}H_{10}F_7NO_6S_4$, *Mr* = 621.53, Triclinic, P-1, a = 8.6082(10) Å, α = 97.782(2)º, b = 13.6635(16) Å, β = 90.026(2)º, c = 21.298(3) Å, γ = 102.338(2)º, *V* = 2423.5(5) Å^3, Z = 4, R1 = 0.0672, wR2 = 0.1771, *T* = 300(2) K. **18**. $C_{23}H_{12}F_3NO_6S_4$, *Mr* = 583.62, Triclinic, P-1, a = 7.9267(15) Å, α = 85.534(3)º, b = 8.4428(16) Å, β = 78.675(3)º, c = 18.761(3) Å, γ = 76.174(3)º, *V* = 1194.8(4) Å^3, Z = 2, R1 = 0.0542, wR2 = 0.1429, *T* = 300(2) K.

Device preparation and characterization. The devices were prepared by using a bottom gate top contact graphite electrodes on highly n^{++} doped silicon substrates with 200 nm of thermally grown silicon dioxide. The source and drain graphite electrodes were prepared by drawing with graphite paste the electrodes on the crystal previously grown on the oxidized silicon wafer. The crystals were formed in all cases by drop casting a drop of a chlorobenzene or toluene solution on the substrate and allowing the solvent to evaporate slowly in the dark at room temperature. Electrical characterization was carried out under ambient conditions (*T* = 24-26ºC and RH = 45-55%) and darkness using a Probe-station from Süss MicroTech and a Keithley 2612A SourceMeter. A homemade Matlab-program using Instrument Control Toolbox 2.0 was used to measure the current-voltage characteristics. Field-effect mobilities were extracted in the saturation regime from the transfer characteristics using the formula:[35]

$$\mu_{FE,sat} = \frac{2 \cdot L}{W \cdot C_i} \cdot \left(\frac{\partial \sqrt{I_{D,sat}}}{\partial V_G} \right)^2_{V_D=const}$$

Here $\mu_{FE,sat}$ is the mobility, C_i the insulator capacitance per unit area, and W and L the width and length of the crystal between the electrodes, respectively. The effective channel width *W* was determined by optical microscopy (see Figure 5).

Acknowledgements

The authors thank the support of EU by the EC FP7 ONE-P large-scale project (no. 212311), Marie Curie EST FuMASSEC, DGI, Spain (contract CTQ2006-06333/BQU) and the programme "Juan de la Cierva"(MICINN). We also thank Stefan T. Bromley for his advice regarding the DFT calculations and CESGA for the use of their instalations. The work in Mons is also supported by the European ONE-P project as well as by the Belgian National Fund for Scientific Research (FNRS). Y.O. and J.C. are FNRS research fellows.

Supporting Information Available: Contains NMR spectra of the prepared compounds, electrochemical, UV-Vis and XRD data. This material is available free of charge via the Internet at http://pubs.acs.org.

Notes and references

1 a) Wudl, F.; Smith, G.M.; Hufnagel, E. J. *J. Chem. Soc., Chem. Commun.*, **1970**, 1453-1454. b) Coffen, D. L.; Chambers, J. Q.; Williams, D. R.; Garrett, P. E.; Canfield, N. D. *J. Am. Chem. Soc.*, **1971**, *93*, 2258–2268. c) Hünig, S.; Kiesslich, G.; Sceutzow, D.; Zhrandik, R.; Carsky, P. *Int. J. Sulfur Chem.*, *Part C*, **1971**, 109.

2 See review papers in the issue Chem. Rev., **2004**, 104.

3 a) Mas-Torrent, M.; Rovira, C. *J. Mater. Chem.*, **2006**, *16*, 433-436. b) Mas-Torrent, M.; Hadley, P.; Bromley, S. T.; Ribas, X.; Tarrés, J.; Mas, M.; Molins, E.; Veciana, J.; Rovira, C. *J. Am. Chem. Soc.*, **2004**, *126*, 8546-8553. c) Mas-Torrent, M.; Durkut, M.; Hadley, P.; Ribas, X.; Rovira, C. *J. Am. Chem. Soc.,* **2004**, *126*, 984-985. d) Bromley, S. T.; Mas-Torrent, M.; Hadley, P.; Rovira, C. *J. Am. Chem. Soc.*, **2004**, *126*, 6544-6545.

4 Leufgen, M.; Rost, O.; Gould, C.; Schmidt, G.; Geurts, J.; Molenkamp, L. W.; Oxtoby, N. S.; Mas-Torrent, M.; Crivillers, N.; Veciana, J.; Rovira, C. *Organic Electronics*, **2008**, *9*, 1101-1106.

5 Takahashi, Y.; Hasegawa, T.; Horiuchi, S.; Kumai, R.; Tokura, Y.; Saito, G. *Chem. Mater.*, **2007**, *19*, 6382-6384.

6 Mas-Torrent, M.; Hadley, P.; Bromley, S. T.; Crivillers, N.; Veciana, J.; Rovira, C. *Appl. Phys. Lett.*, **2005**, *86*, 012110/1-012110/3.

7 a) Naraso; Nishida, J.-I.; Ando, S.; Yamaguchi, J.; Itaka, K.; Koinuma, H.; Tada, H.; Tokito, S.; Yamashita, Y. *J. Am. Chem. Soc.*, **2005**, *127*, 10142-10143. b) Naraso; Nishida, J.-I.; Kumaki, D.; Tokito, S.; Yamashita, Y. *J. Am. Chem. Soc.*, **2006**, *128*, 9598-9599.

8 a) Gao, X.; Wu, W.; Liu, Y.; Qiu, W.; Sun, X.; Yu, G.; Zhu, D. *Chem. Commun.*, **2006**, 2750-2752; b) Noda, B.; Katsuhara, M.; Aoyagi, I.; Mori, T.; Taguchi, T. *Chem. Lett.*, **2005**, *34*, 392-393.

9 Gao, X.; Wang, Y.; Yang, X.; Liu, Y.; Qiu, W.; Wu, W.; Zhang, H.; Qi, T.; Liu, Y.; Lu, K.; Du, C.; Shuai, Z.; Yu, G.; Zhu, D. *Adv. Mater.*, **2007**, *19*, 3037-3042.

10 a) Hoshino, S.; Toshida, M.; Uemura, S.; Kodzasa, T.; Takada, N.; Kamata, T.; Yase, K. *J. Appl. Phys.*, **2004**, *95*, 5088-5093. b) Abdou, M. S. A.; Lu, X.; Xie, Z. W.; Orfino, F.; Deen, M. J. Holdcroft, S. *Chem. Mater*, **1995**, *7*, 631-641. c) Abdou, M. S. A.; Orfino, F. P.; Son, Y.; Holdcroft, S. *J. Am. Chem. Soc.*, **1997**, *119*, 4518-4524. d) Aguirre, C. M.; Levesque, P. L.; Paillet, M.; Lapointe, F.; St-Antoine, B. C.; Desjardins; P.; Martel, R. *Adv. Mater.*, **2009**, *21*, 3087-3091.

11 a) Almlöf, J. E.; Feyereisen, N. W.; Jozefiak, T. H.; Miller, L. L. *J. Am. Chem. Soc.*, **1990**, *112*, 1206-1214. b) Stanton, F. R.; Jozefiak, T. H.; Miller, L. L. *J. Org. Chem.*, **1990**, *55*, 4794-4801. c) Stanton, F. R.; Miller, L. L. *J. Am. Chem. Soc.*, **1992**, *114*, 1388-1394. d) Dumur, F.; Gautier, N.; Gallego-Planas, N.; Sahin, Y.; Levillain, E.; Mercier, N.; Hudhomme, P. *J. Org. Chem.*, **2004**, *69*, 2164-2177. e) Chen, M.-C.; Kim, C.; Chen, S.-Y.; Chiang, Y.-J.; Chung, M.-C.; Facchetti, A.; Marks, T. J.; *J. Mater. Chem.*, **2008**, *18*, 1029-1036.

12 a) Llacay, J.; Mata, I.; Molins, E.; Veciana, J.; Rovira, C. *Adv. Mater.*, **1998**, *3*, 330-334. b) Baffreau, J.; Dumur, F.; Hudhomme, P. *Org. Lett.*, **2006**, *8*, 1307-1310.

13 Reddy, P. Y.; Kondo, S.; Toru, T.; Ueno, Y. *J. Org. Chem.*, **1997**, *62*, 2652-2654.

14 Crivillers, N.; Oxtoby, N. S.; Mas-Torrent, M.; Veciana, J.; Rovira, C. *Synthesis*, **2007**, *11*, 1621-1623.

15 a) Bando, Y.; Shirahata, T.; Shibata, K.; Wada, H.; Mori, T.; Imakubo, T. *Chem. Mater.*, **2008**, *20*, 5119-5121. b) Yan, Q.; Zhou, Y.; Ni, B.-B.; Ma, Y.; Wang, J.; Pei, J.; Cao, Y. *J. Org. Chem.*, **2008**, *73*, 5328-5339. c) Tang, M. L.; Reichardt, A. D.; Siegrist, T.; Mannsfeld, S. C. B.; Bao, Z. *Chem. Mater.*, **2008**, *20*, 4669-4676. d) Son, H.-J.; Han, W.-S.; Chun, J.-Y.; Kwon, S.-N.; Ko, J.; Kang, S. O.; *Organometallics*, **2008**, *27*, 2464-2473.

16 a) Viruela, R.; Viruela, P. M.; Pou-Amérigo, R.; Ortí, E. *Synthetic Metals*, **1999**, *103*, 1991-1992. b) Berridge, R.; Serebryakov, I. M.; Skabara, P. J.; Ortí, E.; Viruela, R.; Pou-Amérigo, R.; Coles, S. J.; Hursthouse, M. B. *J. Mater. Chem.*, **2004**, *14*, 2822-2830. c) Terkia-Derdra, N.; Andreu, R.; Sallé, M.; Levillain, E.; Orduna, J.; Garín, J.; Ortí, E.; Viruela, R.; Pou-Amérigo, R.; Sahraoui, B.; Gorgues, A.; Favard, J.-F.; Riou, A. *Chem. Eur. J.*, **2000**, *6*, 1199-1213.

17 a) Desiraju, G. R. *Acc. Chem. Res.*, **1991**, *24*, 290-296. b) Desiraju, G. R. *Acc. Chem. Res.*, **1996**, *29*, 441-449. c) Steiner, T.; Desiraju, G. R. *Chem .Commun.*, **1998**, 891-892.

18 Crivillers, N.; Mas-Torrent, M.; Bromley, S. T.; Wurst, K.; Veciana, J.; Rovira, C. *ChemPhysChem*., **2007**, *8*, 1565-1571.

19 Troisi, A.; Orlandi, G. *Phys. Rev. Lett.*, **2006**, *96*, 86601.

20 Jortner, J. *J. Chem. Phys.*, **1976**, *64*, 4860-4867.

21 a) Valeev, E. F.; Coropceanu, V.; da Silva, D. A.; Salman, S.; Brédas, J.-L. *J. Am. Chem. Soc.*, **2006**, *128*, 9882-9886. b) Senthilkumar, K.; Grozema, F. C.; Bickelhaupt, F. M.; Siebbeles, L. D. A. *J. Chem. Phys.*, **2003**, *119*, 9809-9817.

22 Coropceanu, V.; Cornil, J.; da Silva Filho, D. A.; Olivier, Y.; Silbey, R.; Brédas, J.-L. *Chem. Rev.*, **2007**, *107*, 926-952.

23 Coropceanu, V.; Malagoli, M.; da Silva Filho, D. A.; Gruhn, N. E.; Bill, T. G.; Brédas, J. L. *Phys. Rev. Lett.*, **2002**, *89*, 275503.

24 Marcus, R. A. *J. Chem. Phys.*, **1965**, *43*, 679-701.

25 Lemaur, V.; da Silva Filho, D. A.; Coropceanu, V.; Lehmann, M.; Geerts, Y.; Piris, J.; Debije, M. G.; van de Craats, A. M.; Senthilkumar, K.; Siebbeles, L. D. A.; Warman, J. M.; Brédas, J. L.; Cornil, J. *J. Am. Chem. Soc.*, **2004**, *126*, 3271-3279.

26 Bromley, S. T.; Illas, F.; Mas-Torrent, M. *Phys. Chem. Chem. Phys.*, **2008**, *10*, 121-127.

27 a) Brédas, J. L.; Calbert, J. P.; da Silva Filho, D. A.; and Cornil, J. *Proc. Nat. Acad. Sci. USA*, **2002**, *99*, 5804. b) Brédas, J. L.; Beljonne, D.; Coropceanu, V.; Cornil, J. *Chem. Rev.*, **2004**, *104*, 4971-5004.

28 Reese, C.; Bao, Z. *Adv. Mat.*, **2007**, *19*, 4535-4538. b) Sundar, V. C.; Zaumseil, J.; Podzorov, V.; Menard, E.; Willett, R. L.; Someya, T.; Gershenson, M. E.; Rogers, J. A. *Science*, **2004**, *303*, 1644-1646. c) Lee, J. Y.; Roth, S.; Park, Y. W. *Appl. Phys. Lett.*, **2006**, *88*, 252106.

29 Olivier, Y.; Lemaur, V.; Brédas J.-L.; Cornil, J. *J. Phys. Chem. A*, **2006**, *110*, 6356-6364.

30 a) Coropceanu, V.; Cornil, J.; da Silva Filho, D. A.; Olivier, Y.; Silbey, R.; Brédas, J.-L., *Chem. Rev.*, **2007**, *107*, 926-952. b) Brédas, J.-L.; Beljonne, D.; Coropceanu, V.; Cornil, J., *Chem. Rev.*, **2004**, *104*, 4971-5004.

31 Rovira, C. *Chem. Rev.*, **2004**, *104*, 5289-5317.

32 Brillante, A.; Bilotti, I.; Della Valle, R. G.; Venuti, E.; Milita, S.; Dionigi, C.; Borgatti, F.; Lazar, A. N.; Biscarini, F.; Mas-Torrent, M.; Oxtoby, N. S.; Crivillers, N.; Veciana, J.; Rovira, C.; Leufgen, M.; Schmidt, G.; Molenkamp, L. W. *CrystEngComm*, **2008**, *10*, 1899-1909.

33 Gaussian 03, Revision E01; Frisch, M. J.; Trucks, G. W.; Schlegel, H. B.; Scuseria, G. E.; Robb, M. A.; Cheeseman, J. R.; Montgomery, J. J. A.; Vreven, T.; Kudin, K. N.; Burant, J. C.; Millam, J. M.; Iyengar, S. S.; Tomasi, J.; Barone, V.; Mennucci, B.; Cossi, M.; Scalmani, G.; Rega, N.; Petersson, G. A.; Nakatsuji, H.; Hada, M.; Ehara, M.; Toyota, K.; Fukuda, R.; Hasegawa, J.; Ishida, M.; Nakajima, T.; Honda, Y.; Kitao, O.; Nakai, H.; Klene, M.; Li, X.; Knox, J. E.; Hratchian, H. P.; Cross, J. B.; Bakken, V.; Adamo, C.; Jaramillo, J.; Gomperts, R.; Stratmann, R. E.; Yazyev, O.; Austin, A. J.; Cammi, R.; Pomelli, C.; Ochterski, J. W.; Ayala, P. Y.; Morokuma, K.; Voth, G. A.; Salvador, P.; Dannenberg, J. J.; Zakrzewski, V. G.; Dapprich, S.; Daniels, A. D.; Strain, M. C.; Farkas, O.; Malick, D. K.; Rabuck, A. D.; Raghavachari, K.; Foresman, J. B.; Ortiz, J. V.; Cui, Q.; Baboul, A. G.; Clifford, S.; Cioslowski, J.; Stefanov, B. B.; Liu, G.; Liashenko, A.; Piskorz, P.; Komaromi, I.; Martin, R. L.; Fox, D. J.; Keith, T.; Al-Laham, M. A.; Peng, C. Y.; Nanayakkara, A.; Challacombe, M.; Gill, P. M. W.; Johnson, B.; Chen, W.; Wong, M. W.; Gonzalez, C.; Pople, J. A.; Gaussian, Inc., Wallingford CT: **2004**.

34 Bartolottiand, L. J.; Fluchick, K. *Reviews in Computational Chemistry*; VCH: New York, **1996**; Vol. 7.

35 Horowitz, G.; Hajlaoui, R.; Bouchriha, H.; Bourguiga, R.; Hajlaoui, M. *Adv. Mater.*, **1998**, *10*, 923-927.

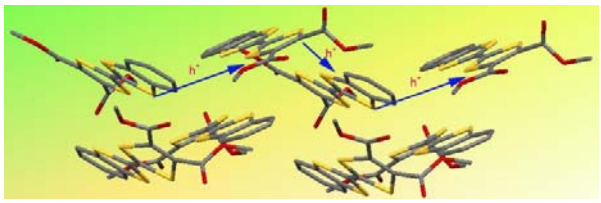

The attachment of phthalimide and carbomethoxy groups to the TTF skeleton increases their electron affinity and solubility allowing for the preparation of air-stable OFETs from solution.